Earth and Planetary Science Letters 522 (2019) 12–19

Contents lists available at ScienceDirect

Earth and Planetary Science Letters

www.elsevier.com/locate/epsl

Deciphering the atmospheric signal in marine sulfate oxygen isotope composition ☆

A.R. Waldeck *, B.R. Cowie, E. Bertran, B.A. Wing, I. Halevy, D.T. Johnston

ARTICLE INFO

Article history:
Received 11 September 2018
Received in revised form 22 May 2019
Accepted 13 June 2019
Available online 1 July 2019
Editor: L. Derry

Keywords:
triple oxygen isotopes
sulfate
sulfate reduction
atmospheric composition

ABSTRACT

Atmospheric O_2 and CO_2 levels inform us of the changes in chemical and biological environments, yet the history of atmospheric compositions, and pO_2 in particular, is not well-constrained. The triple oxygen isotope ($^{16,17,18}O$) composition of marine SO_4^{2-} has been proposed to directly record the ratio pO_2/pCO_2 in the contemporaneous atmosphere. To resolve this atmospheric signal, both a precise measurement of the ^{17}O composition of sulfate and a model with which to interpret the measurement are needed. Here we present precise measurements of the triple oxygen isotope composition of modern marine sulfate and then forward a novel sulfur cycle model that deconvolves the potential atmospheric and microbial inputs to this signal. Our interpretation of marine sulfate oxygen isotope composition provides a framework for calculating atmospheric composition, relative rates of biogeochemical activity, and can be applied to geologic records of marine sulfate to constrain the pO_2/pCO_2 ratio over time.

1. Introduction

Atmospheric composition has evolved throughout the Phanerozoic (542 million years to present), with data informed model estimates serving as the gold standard for the presumed histories of pO_2 and pCO_2 (Berner, 2006; Bergman et al., 2004). These models fundamentally differ in their predictions for when and how the evolution of land plants influenced Phanerozoic pO_2. This difference is one example that reveals a need for direct method of determining past pO_2 and pCO_2. No geochemical proxy record can directly access the evolution of the Phanerozoic atmosphere, however the ^{17}O composition of seawater sulfate may provide such a window (Bao et al., 2009, 2008).

Seawater sulfate ^{17}O composition is increasingly used as a tool for assaying atmospheric composition on the Precambrian Earth. As interpreted in the Precambrian (Bao et al., 2008, 2009; Crockford et al., 2016), the sulfate produced by oxidative weathering in terrestrial environments carries a much lower $^{17}O/^{16}O$ than would be predicted from $^{18}O/^{16}O$ (that is, it can be mass-independent). The $>1‰$ (parts per thousand) depletion observed in ^{17}O relative to ^{18}O from ancient sulfate minerals (Bao et al., 2008, 2009) is interpreted as being derived from reactions that generate and consume O_2 in the atmosphere, and the magnitude of this depletion proportional to the relative amounts of O_2 and CO_2 gases in the stratosphere. This O_2 isotopic signal is assumed to be incorporated into sulfate during oxidative pyrite weathering (Killingsworth et al., 2018). Riverine sulfate then carries a mass-independent isotopic composition reflective of atmospheric O_2 isotopic composition. Excluded from these interpretations is marine biogeochemistry. Biological reactions within marine sediments today produce sulfate as a metabolite with a different oxygen isotopic composition than the riverine contribution. Here, sulfate produced from microbial reactions has a ratio $^{17}O/^{16}O$ that correlates with its ratio of $^{18}O/^{16}O$ (is mass-dependent) and is linked to the oxygen isotopic composition of seawater. Thus, biological reactions counteract the ^{17}O anomaly imparted from the atmosphere during oxidative weathering, and the degree to which this occurs is determined by the relative magnitude of sulfate contributions from rivers to biological cycling. Developing quantitatively accurate models for these fluxes and their impact on marine sulfate budgets is vital for the interpretation of ancient sulfate and climate records.

The largest sulfate input to the oceans is thought to be from the oxidative weathering of terrestrial sulfides and dissolution of evaporites ($CaSO_4$), with delivery via rivers (Halevy et al., 2012; Wortmann et al., 2007). Sulfate is then removed from the ocean through biological reactions and precipitation of sedimentary sulfides and sulfates (evaporites, anhydrite, and carbonate associated sulfate). In the modern environment, sulfate is the second most abundant anion in seawater and carries three times the oxidizing capacity of atmospheric oxygen (Hayes and Waldbauer, 2006). It then follows that many metabolisms derive energy from sulfur reduction-oxidation reactions (Canfield, 2004). The oxidation of

☆ We thank K. Casciotti and W. Berelson for sample collection (Johnston et al., 2014). Funding was provided by Harvard University (A.W.), NSF OCE-1821958, and NASA NNA13AA90A and NNX15AP58G.

* Corresponding author.
E-mail address: waldeck@g.harvard.edu (A.R. Waldeck).

https://doi.org/10.1016/j.epsl.2019.06.013
0012-821X/

sulfides and/or reduction of sulfate through any of these processes is often rapid, biologically mediated, and carries distinct isotopic consequences. More specifically, biological reactions like microbial sulfate reduction (MSR) allow for exchange of the oxygen atoms in sulfate with oxygen atoms in water (Wankel et al., 2014). Though there may be no net removal of sulfur from the environment, there remains the opportunity for the oxygen isotope composition of sulfate to be reset through this cycling (Turchyn and Schrag, 2004). Processes affecting the oxygen isotopic composition of sulfate are thus integrated across the residence time of oxygen atoms in the dissolved sulfate molecule, with previous estimates of this residence time based just on sulfide oxidation rates and weathering fluxes on the order of 1 million years for the oxygen atoms within sulfate (Turchyn and Schrag, 2004), versus 10 million years for the sulfur atom within sulfate (Paytan et al., 2004, 1998).

In parallel to flux magnitudes, understanding the marine sulfate reservoir requires knowledge of the isotope effects of these fluxes. Fortunately, global (modern) riverine sulfate isotopic compositions have been measured (see SOM, Section 8.4), however the biological sulfate $^{18}O/^{16}O$ effect is more difficult to constrain. Environmental and laboratory studies point to the capacity for different microorganisms to generate a variety of $^{18}O/^{16}O$ ratios during biological cycling of sulfate (Fritz et al., 1989; Böttcher and Thamdrup, 2001; Böttcher et al., 2001; Brunner and Bernasconi, 2005; Turchyn et al., 2010). An alternative approach assumes that pore water sulfates capture all the relevant biogeochemical and physical processes (Antler et al., 2013, 2015) and their study can be used to calibrate the $^{18}O/^{16}O$ ratio. This approach includes key inorganic equilibria between water, sulfur, and phosphorus intermediate species that may play a critical role in setting the composition of the ocean (Wankel et al., 2014; Müller et al., 2013; Zeebe, 2010). While $^{18}O/^{16}O$ isotope effect studies continue to prove valuable and gain complexity (Bertran et al., 2019), unraveling these complex systems is facilitated with the added constraint of $^{17}O/^{16}O$ composition.

Here we use the multiple oxygen isotope (^{16}O, ^{17}O, ^{18}O) composition of modern seawater sulfate in combination with a new theoretical framework to constrain key sulfur cycle fluxes in the modern. The ^{17}O composition of modern marine sulfate is herein measured in four one-dimensional water column profiles: two long-term time series sites (BATS and SAFE), and two profiles through the oxygen minimum zone in the Eastern Tropical South Pacific (ETSP station 5 and 11). These measurements are enabled via a new analytical method for measuring oxygen isotopes in sulfate (Cowie and Johnston, 2016). To interpret an individual isotope composition of modern marine sulfate, we describe the data as a mixture of two competing fluxes: weathering and marine biological recycling. This new model framework and expanded consideration of sulfate ^{17}O composition enables the interpretation of the modern sulfate oxygen isotope composition and provides an improved framework for evaluating geological records.

2. Nomenclature

Throughout this work we use standard $\delta^{18}O$ notation for reporting $^{18}O/^{16}O$ ratios. This notation is consistent with other water buffered systems (i.e. $CaCO_3$) and paleoclimate studies (Zeebe and Wolf-Gladrow, 2001). Isotope ratios are reported as the abundance of a heavy isotope divided by the abundance of the lighter, most abundant isotope. The isotope ratio of a sample (e.g. $^{18}R_{\text{sample}}$) is compared to the isotope ratio of a known reference material, here Vienna Standard Mean Ocean Water (VSMOW), and thus $\delta^{18}O$ is defined as:

$$\delta^{18}O = 10^3\left(\frac{^{18}R_{\text{sample}}}{^{18}R_{\text{VSMOW}}} - 1\right), \tag{1}$$

where the units are parts per thousand, or "permil" (‰). The ratio $^{17}O/^{16}O$ and $\delta^{17}O$ are calculated analogously.

Processes that isotopically fractionate materials are described by a fractionation factor α. For a process or relationship between two compositions (A and B), $^{1x}\alpha$ ($= {}^{1x}R_A/{}^{1x}R_B$). For a mass-dependent process,

$$^{17}\alpha = (^{18}\alpha)^{\theta} \tag{2}$$

where θ is a value close to 0.5, but can range from 0.516 to 0.531 depending on the process (Landais et al., 2008; Barkan and Luz, 2005; Pack and Herwartz, 2014; Levin et al., 2014). The calculated high-temperature, mass-dependent triple isotope fractionation at equilibrium is $\theta = 0.5305$ (Cao and Liu, 2011). For a given sample, $\Delta'^{17}O$ is a measure of the deviation of the $^{17}O/^{16}O$ ratio from that predicted by the $^{18}O/^{16}O$ ratio and θ_{RL}.

$$\Delta'^{17}O = 10^6\left(ln\left(\frac{^{17}R_{\text{sample}}}{^{17}R_{\text{VSMOW}}}\right) - \theta_{RL} \times ln\left(\frac{^{18}R_{\text{sample}}}{^{18}R_{\text{VSMOW}}}\right)\right), \tag{3}$$

where the units are parts per million, or "per meg". In keeping with previous work (Pack and Herwartz, 2014; Cao and Liu, 2011; Levin et al., 2014), we use the value 0.5305 as the θ_{RL} (*R*eference *L*ine) in the definition of $\Delta'^{17}O$. Other studies have extended this definition even further, to include non-zero intercepts in $\delta^{17}O$-$\delta^{18}O$ for a chosen reference line (Levin et al., 2014). This term, often noted as γ_{RL}, is an additive property in ‰ units. In this work we chose a reference frame tied to VSMOW and set $\gamma_{RL} = 0$‰. Our in-house VSMOW composition was calibrated based on known silicate standards (Cowie and Johnston, 2016).

3. Methods

Modern seawater sulfate samples were collected from the well-characterized oceanographic sites: BATS (Bermuda-Atlantic Time Series Site), SAFE, and ETSP (Eastern Tropical South Pacific) stations 5 and 11, across a range of depths. Complementary metadata is provided in Johnston et al. (2014). All samples were processed through an established chemical protocol that was thoroughly calibrated with sulfate standard materials (Johnston et al., 2014; Cowie and Johnston, 2016). First, all water column sulfate samples were precipitated as barite. Further purification of precipitates was achieved via dissolution and reprecipitation by addition of a 0.05 M solution of diethylenetriaminepentaacetic acid (DTPA) and base (1 M NaOH). Re-precipitation was achieved upon addition of HCl to pH<3, after which the solution was centrifuged, supernatant decanted, and residual barite dried for 24 h at 110 °C. This further chemical step ensures that only $BaSO_4$ is present in the precipitate. Note that the oxygen isotope exchange between sulfate and water occurs with an extremely long half-life (>10^5 h at 25 °C and pH 1 (Rennie and Turchyn, 2014)).

The $\delta^{18}O$ value of sulfate was first measured by High-Temperature Conversion Elemental Analyzer (TC/EA) techniques. Here, 400±50 µg of barite powder was loaded into silver cups with excess glassy carbon for analysis on a TC/EA connected to a Thermo Scientific Delta V Plus isotope ratio mass spectrometer configured in continuous flow mode. The combustion generates CO as the analyte gas. All samples were analyzed in at least triplicate, and raw data were normalized to the accepted values for international standards IAEA-SO-5, IAEA-SO-6, and NBS-127 (see Johnston et al., 2014; Cowie and Johnston, 2016 for standardization and corrections of IAEA standards). Instrument precision for $\delta^{18}O$ by TC/EA was < 0.3‰ (1σ), and the data were originally reported in Johnston et al. (2014).

Measuring the triple isotope composition of sulfate required fluorination of barite to generate O_2. We recently developed and

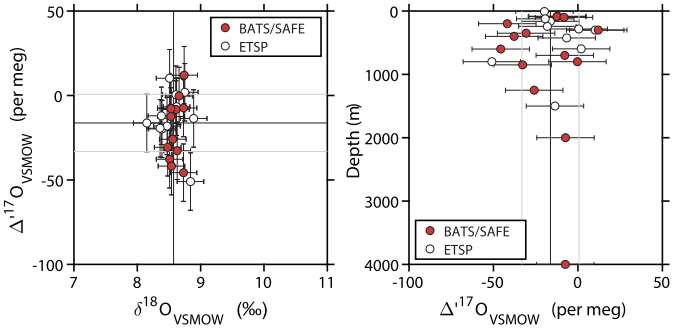

Fig. 1. Measurements of marine sulfate ^{18}O and ^{17}O isotopic composition from two locations: Bermuda Atlantic Time-series Study (BATS) (red filled circles) and Eastern Tropical South Pacific (ETSP, sites 5 and 11) (open circles). Sulfate compositions are $\delta^{18}O = +8.67 \pm 0.21‰$ and $\Delta'^{17}O = -16 \pm 17$ per meg ($-0.016‰$). The left panel depicts both $\Delta'^{17}O$ (y-axis) and $\delta^{18}O$ (x-axis) compositions of marine sulfate; the right panel confirms that the $\Delta'^{17}O$ composition (x-axis) does not vary significantly with depth (y-axis). (For interpretation of the colors in the figure(s), the reader is referred to the web version of this article.)

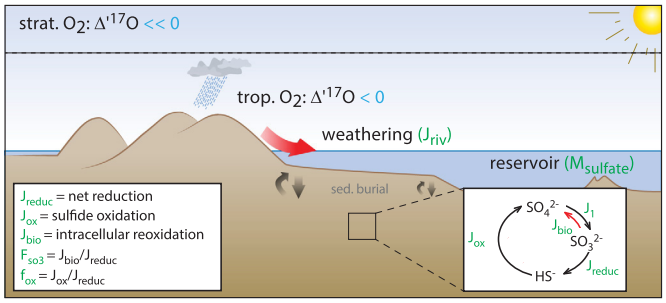

Fig. 2. Schematic of the sulfur cycle with its four main fluxes: weathering J_{riv}, sulfate reduction J_{reduc}, pyrite burial J_{py}, and reoxidation processes (J_{bio}, J_{ox}). The atmospheric anomaly (strat O_2 $\Delta'^{17}O \ll 0$) passes to ocean sulfate via J_{riv}. Subsequent microbial and abiotic reactions (J_{ox}, J_{bio}) reset the O isotope composition of sulfate.

calibrated a new method (Cowie and Johnston, 2016) for measuring the triple oxygen isotope composition of sulfate minerals, requiring $\approx$ 2 mg of barite, using fluorine gas (F_2) and a 50 W infrared laser to generate analyte O_2. Once O_2 is generated, the analyte gas is purified via numerous cryofocus steps and the introduction of an in-line gas chromatograph (GC). We fraction collect the sample post-GC, quantify our yields via peak integration, and pass clean O_2 through to a Thermo Scientific MAT 253 in dual-inlet mode. As with previous methods, our fluorination technique still requires pairing with independent $\delta^{18}O$ measurements made by TC/EA. To determine $\Delta'^{17}O$, or the ^{17}O composition relative to the ^{18}O composition of the sample, a correction is applied that accounts for the fluorination yield and fractionation therein (Cowie and Johnston, 2016). This correction for the mass-dependent isotope effect observed during barite fluorination was rigorously calibrated (as a function of O_2 yields) and is now available for the treatment of environmental data sets like that presented herein.

4. Results

The oxygen isotope composition of modern marine sulfate is statistically homogeneous, with a value of $\delta^{18}O_{VSMOW} = +8.67 \pm 0.21‰$ (see Johnston et al., 2014). New measurements presented here illustrate that $\Delta'^{17}O_{VSMOW}$ is similarly homogeneous with a composition of $-0.016 \pm 0.017‰$ (see Fig. 1). This is also true in oxygen minimum zones, where some degree of cryptic sulfur cycling may occur (Canfield et al., 2010; Johnston et al., 2014). Moreover, this observation is consistent with the long residence time of sulfate oxygen in the ocean relative to oceanic mixing (Turchyn and Schrag, 2004). As noted above, these data are derived from four, 1-D water column profiles in major ocean basins (Tables S2 and S3). These include two classic time series sites (BATS and SAFE) and two profiles through OMZ-bearing water columns, ETSP stations 5 and 11 - the same localities used in the $\delta^{18}O_{VSMOW}$ calibration of marine sulfate. As Fig. 1 shows, samples from different column profiles have $\Delta'^{17}O_{VSMOW}$ values that are the same within statistical error. Further interrogation of the information locked within the $\Delta'^{17}O_{VSMOW}$ composition thus requires an understanding of the behavior of ^{17}O within the sulfur cycle.

5. Model

Previous models of seawater sulfate account for the modern composition and temporal variability in oxygen isotope distribution in sulfate by changing the size and isotope composition of the input and output fluxes to the seawater sulfate reservoir (Turchyn and Schrag, 2004, 2006). Using mass balance, these fluxes are either set to accommodate the composition of the modern ocean or modified to exert the required rate of isotopic change to satisfy the empirical record, while accounting for the net change in the size of the marine sulfate reservoir. The models are commonly constrained by four fluxes (refer to Fig. 2). First, sulfate enters the ocean via rivers (J_{riv}) that contain sulfate from the continental weathering of evaporites and oxidation of pyrite minerals. Once in the ocean, most sulfate is removed through dissimilatory sulfate reduction (J_{reduc}). This metabolism, largely located within organic-rich continental shelf sediments, transforms sulfate into sulfide through a series of intermediate reaction steps. Some of the sulfide produced (J_{reduc}) is immediately re-oxidized to sulfate (J_{ox}), and the re-oxidized fraction is denoted as f_{ox} (or J_{ox}/J_{reduc}) (Jørgensen, 1982). The remaining biogenic sulfide ($[1\text{-}f_{ox}]\cdot J_{reduc}$) reacts with iron and precipitates as pyrite in the sediments. Although these fluxes constitute the bulk of the sulfur cycle, secondary sulfur sinks could be important and include the precipitation of anhydrite ($CaSO_4$) and sulfide minerals (largely FeS_2) in hydrothermal settings. Each flux within the sulfur cycle carries an associated isotope effect, which is empirically derived in almost all cases. Isotopic variability in the environment introduces further uncertainty into these estimates. For instance, riverine sulfate oxygen isotope composition varies spatially as a function of the terrain it is draining. This can relate to the proportions of weathered evaporite and oxidized pyrite minerals (see Fig. S4 & S5). More loosely constrained, the isotopic signatures of microbial sulfate reduction and sulfide oxidation appear prominently in previous models, but are not tied to the likely significant local environmental conditions.

This work evaluates the multiple oxygen isotope compositions (^{18}O and ^{17}O) of global seawater sulfate as a sum of two processes: (1) riverine sulfate input to the ocean and (2) biological (i.e. microbial) recycling of sulfate within the ocean system. Here we define marine sulfate to include the water column and pore waters within diffusive reach of the seawater pool. We define sulfate recycling as including the sulfate generated via reoxidation within sulfate reducing microorganisms (J_{bio}) rather than canonical sulfide oxidation (J_{ox}) (see Fig. 2).

5.1. Riverine sulfate isotope composition

Oxidative weathering of pyrite and dissolution of evaporite minerals in terrestrial environments sets the composition of riverine sulfate. It follows that the protolith, or terrain being weathered, exerts a prominent control on marine sulfate isotope composition. Isotopically depleted sulfate often indicates a higher contribution from weathered pyrite (FeS_2), whereas more enriched $\delta^{18}O$ values indicate an increased contribution from weathered evaporite minerals ($CaSO_4$). Previous models have used an intermediate value for $\delta^{18}O$ of riverine sulfate to capture this mixing behavior, using an

Table 1
These are the constraints on the ranges of each of the model parameters, summarized from the text. Citations: [1] (Turchyn and Schrag, 2004) and *ref* therein, [2] (Farquhar et al., 2008), [3] see SOM section 8.4, [4] (Killingsworth et al., 2018), [5] (Bertran et al., 2019), [6] (Cao and Liu, 2011), [7] prelim. data, Johnston Lab, see SOM section 8.2.

Variable	min	max	Units	References
$\log(J_{riv}/J_{bio})$	−1.1	−0.7	–	[1,2]
$\delta^{18}O_{riv}$	+1.2	+10.9	‰	[3]
$\Delta'^{17}O_{riv}$	−200	0	per meg	[4]
$\delta^{18}O_{bio}$	+24	+27	‰	[5]
$^{17}\theta_{bio}$	0.527	0.5305	–	[6,7]

estimated ratio of 2:1 (pyrite:evaporite) and scaled with continental shelf exposure (Turchyn and Schrag, 2006). A more recent sulfur isotope study estimated that weathered pyrite makes up close to 43% of the modern riverine sulfate budget (Burke et al., 2018). In parallel to these estimates, a global compilation illustrates a wide range of potential $\delta^{18}O$ sulfate values, consistent with the wide range of geological terrains being drained. For our model, we use a range of $\delta^{18}O$ from 1.2 to 10.9‰, reflective of the 25th and 75th percentiles from a compilation of 469 published measurements of river sulfate (see SOM, Section 8.4).

The minor oxygen isotope composition of riverine sulfate is poorly constrained. A single study of the Mississippi River sulfate budget suggests an average $\Delta'^{17}O$ of -90 ± 40 per meg (-0.090 ± 0.040‰), which is characteristic of a mass-independent isotope composition (Killingsworth et al., 2018). Like the $\delta^{18}O$ values of sulfate, it is expected that this composition results from two component mixing between oxidative pyrite weathering and evaporite dissolution.

Implicit in all these studies is the degree of oxygen atom transfer between tropospheric O_2 and product sulfate. This fraction has been measured using both ^{18}O-labeling (Van Stempvoort and Krouse, 1994; Tichomirowa and Junghans, 2009) and ^{17}O inclusive (Kohl and Bao, 2011) experiments that suggest that anywhere from 0-50% of the oxygen atoms are derived from O_2, and this proportion is pH and Fe^{3+}-dependent. Given the present isotope composition of tropospheric O_2 ($\Delta'^{17}O = -520$ per meg), and assuming that 100% of the riverine sulfate is derived from pyrite oxidation would yield a river composition between 0 and −260 per meg. Contributions from evaporite dissolution could augment this oxidative signal, and comprehensive, time-dependent constraints on evaporite compositions are still debated in general (Halevy et al., 2012), and fully lacking for ^{17}O. Given these uncertainties, the model calculations that follow allow riverine sulfate compositions to vary widely, across the full range of measured river sulfate $\Delta'^{17}O$, from −200 to 0 per meg. This will be refined as riverine and oxidation studies provide the needed constraints. See Table 1.

5.2. Microbial sulfate isotopic composition

The oxygen isotope composition of marine sulfate captures information from a suite of biological processes that reduce and regenerate sulfate in the ocean. Laboratory experiments on microbial sulfate reduction (MSR) demonstrate that this metabolism leaves the residual sulfate pool isotopically enriched in $\delta^{18}O$ (J_{reduc}), whereas similar work with sulfide oxidation (J_{ox}) produces sulfate with a range of $\delta^{18}O$ values near (or slightly heavier than) ambient water (Van Stempvoort and Krouse, 1994). Both vectors carry uncertainty in isotopic consequences and in material flux. This is especially true for the sulfide oxidation pathway, where debate remains over the vigor of reoxidation (f_{ox} - the fraction of sulfide oxidized - between 0.4 and 0.9) (Jørgensen, 1982; Masterson et al., 2016). In pore waters, the $\delta^{18}O$ of sulfate increases with sulfate consumption - directly implicating the effects of MSR and sulfate uptake. These microbial isotope effects appear to vary widely depending on the specific local conditions and only loose constraints exist for the cellular-scale controls on the isotope effect.

Sulfate reduction metabolism models are used to predict the oxygen isotope composition of the residual sulfate pool. Though local biological effects on sulfate oxygen isotope composition may vary widely, these isotope effects reflect cellular-scale processes and local environmental conditions ($[SO_4^{2-}]$, $[H_2S]$, and pH). This exact constraint was deconvolved for sulfur isotopes (Wing and Halevy, 2014), and more recently for oxygen isotopes (Bertran et al., 2019). For the model described herein, we extract oxygen isotope estimates for typical pore water conditions and rates based on studies of modern pore water sulfate profiles (Burke et al., 2018; Leloup et al., 2009; Hoehler and Jørgensen, 2013). The highest metabolic rates (where most sulfate reduction occurs) found were present at the sediment water interface, and range from 10^{-3} to 0.2 fmol cell^{-1} day^{-1}, scaling with water depth. From the model of Bertran et al. (2019), we obtain an MSR fractionation of $\delta^{18}O \approx$ 24-27‰ ($^{18}\alpha_{bio} = 1.024$-$1.027$).

As previously documented (Farquhar et al., 2008), reoxidative shuttles within sulfate reduction may be the largest biological contributor to extracellular sulfate (in excess when compared to sulfide oxidation). An experiment with isotopically labeled water and a series of sediment flow-through reactors containing sulfate reducers demonstrated that the residual sulfate exiting the reactors had incorporated the isotope label from the ambient water during sulfate reduction. Through measurement of the label incorporation, the calculated magnitude of the sulfite-water exchange and back reaction was $2.33 \cdot J_{reduc}$ (Farquhar et al., 2008). This indicates that intracellular reoxidation exceeds net sulfide production. Using an independent thermodynamic modeling approach, Bertran et al. (2019) calculated the flux of intracellular reoxidative pathways during sulfate reduction. This flux, denoted as F_{SO3}, is the amount of sulfate imported to the cell, partially reduced to sulfite (SO_3^{2-}) and then reoxidized to sulfate and exported from the cell, relative to the amount of sulfate fully reduced to sulfide (Wankel et al., 2014; Bertran et al., 2019):

$$F_{SO_3} = \frac{J_{bio}}{J_{reduc}}. \quad (4)$$

In this model framework, F_{SO_3} varies mainly with cell specific sulfate reduction rate and pore water concentrations of sulfate and sulfide. Values of F_{SO_3} from 0.1-10 are representative of sulfate reduction occurring in the middle to lower sediment column (near the sulfate-methane transition zone) at a rates of 0.1 fmol H_2S/cell·day, and this factor increases exponentially as the rate decreases (see Fig. S6). We define the biological flux (J_{bio}) using the net sulfate reduction flux - as it is used in previous work - augmented by this re-oxidative coefficient ($J_{bio} = J_{reduc} \cdot F_{SO_3}$). J_{bio} is the reoxidation flux *within* a sulfate reducing microorganism. Previous estimates of the modern global rate of microbial sulfate reduction are between 8 and $11.3 \cdot 10^{12}$ mol/yr (Turchyn and Schrag, 2004; Bowles et al., 2014). Combining these estimates with the microbial recycling coefficient yields a microbial oxygen isotope resetting flux between 0.8 and $113.0 \cdot 10^{12}$ mol/yr. Along with the composition of sulfate, our approach will allow for a re-examination of the global sulfate reduction rate.

There have been no published ^{17}O measurements to date on sulfate associated with the sulfate reduction pathway. MSR is a mass-dependent process with respect to sulfur isotopes, with the expectation that this dependence would hold for oxygen. This means that the ^{17}O is predictable given an ^{18}O effect (Barkan and Luz, 2005; Miller, 2002; Young et al., 2002; Landais et al., 2008; Young et al., 2014), although the specific mass law ($^{17}\theta_{bio}$) that describes MSR is largely unknown. Preliminary measurements of

microbial sulfate reduction effects on ^{17}O indicate a $^{17}\theta_{bio}$ value of 0.5285 ± 0.0026 (for preliminary data see SOM). In the discussion that follows, we use this preliminary $^{17}\theta_{bio}$ as a guide, but still allow for a wider range of mass-dependent relationships, from 0.527 to 0.5305.

5.3. Model framework

The isotopic composition of modern seawater sulfate is largely set by riverine sulfate (J_{riv}) and sulfate that is regenerated within the sulfate reduction metabolism (J_{bio}). In a departure from previous models, we approximate that the removal of sulfate (via sulfate reduction, for example) does not significantly affect the isotopic composition of the sulfate reservoir, and therefore do not explicitly include the traditional sulfur output fluxes (i.e. pyrite burial). Instead, the larger biological effect comes from reoxidation within MSR. Intracellular sulfate from this biological flux exchanges oxygen atoms with water, an effectively infinite isotopic reservoir. Further, we choose not to include the traditional J_{ox} flux (oxidation of sulfides), because it is poorly constrained isotopically and is not always significant in magnitude (at conditions representative of average sulfate reduction: csSRR $\leq$ 0.2 fmol cell^{-1} day^{-1} and porewater conditions [SO_4^{2-}] = 10 mM, [H_2S] = 1 mM), F_{SO_3} = 3.1).

Global river fluxes (mol/yr) are estimated either from measured sulfate concentrations in fluvial systems or are based on alkalinity measurements and stoichiometry in continental rocks (Berner and Berner, 2012). These flux estimates vary from 2 to 3.5 · 10^{12} mol/yr for sulfate (Meybeck, 1979). A more recent estimate of 2.8 ± 0.8 · 10^{12} mol/yr is based on sulfate concentration measurements of rivers constituting 46% of global freshwater runoff (Burke et al., 2018). In the modeling that follows, we allow riverine sulfate to vary across this range of values.

6. Discussion

Interpretations of the surface sulfur cycle, whether in the present or past, are limited by the level of constraint on key mechanisms. The size of the modern river sulfate flux has been uniquely determined through field measurements (Burke et al., 2018) and by necessity serves as the anchor point for paleoreconstructions (Turchyn and Schrag, 2004, 2006). Other fluxes (biological, hydrothermal, etc.) are more difficult to directly quantify. For example, the global sulfate reduction rate is often calculated using scaled local reduction rate data (Canfield, 1991; D'Hondt et al., 2002; Niewohner et al., 1998; Thamdrup et al., 1994) and/or compilations of marine profiles (Bowles et al., 2014). Both approaches intrinsically carry more uncertainty than empirical quantities like riverine fluxes. It is in addressing these uncertainties that isotope studies are especially useful.

Because the isotope effects of various sulfate-generating mechanisms overlap, interpreted changes in seawater sulfate $\delta^{34}S$ (as well as ^{33}S and ^{36}S (Masterson et al., 2016)) are non-unique. Sulfur isotope work has shown that riverine sulfate typically ranges in $\delta^{34}S$ from 0 to 10‰ (Holser et al., 1979), and sulfate formed by oxidation of sulfides carries only a small isotope effect (Fry et al., 1988). On the other hand, the isotope fractionation associated with microbial sulfate reduction varies across a wide range, from 0 to 70‰ in $\delta^{34}S$ (Leavitt et al., 2013). Through the model forwarded in this work, we revisit the major fluxes affecting the marine sulfur cycle using both ^{17}O and ^{18}O. This approach is calibrated against the composition of the modern ocean, and extended to geological records.

The $\delta^{18}O$ of modern marine sulfate reflects the relative sulfate fluxes and their respective isotopic compositions. Fig. 3 shows the combination of values for $\delta^{18}O_{riv}$, $\delta^{18}O_{bio}$, and J_{riv}/J_{bio} that are consistent with $\delta^{18}O$ in seawater sulfate of 8.67‰. Imposed on Fig. 3 is a range of $\delta^{18}O$ estimates for modern river systems extrapolated from a compilation of 469 measurements of the $\delta^{18}O$ composition of modern river sulfate. Using the estimate for biological contributions (24.0-27.0‰) (Bertran et al., 2019) and a modern J_{riv}, we solve for a contemporary J_{riv}/J_{bio} value >2.0 that satisfies the ^{18}O composition of the modern ocean (see Fig. 4, left panel, and Fig. 3).

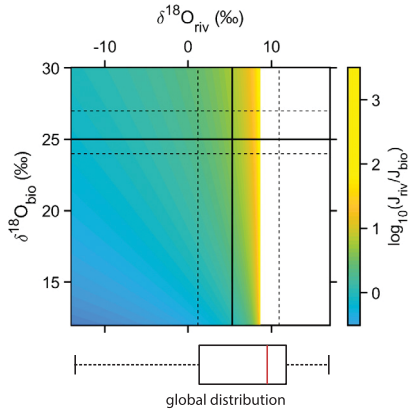

Fig. 3. The space of solutions for modern seawater sulfate ^{18}O-composition is shown here. The log of the ratio of riverine to biological fluxes (colorbar), varies as a function of riverine sulfate ^{18}O-composition (x-axis) and biologically-recycled sulfate ^{18}O-composition (y-axis). The solid black lines indicate the independent estimates for $\delta^{18}O_{bio}$ (25.0‰) and $\delta^{18}O_{riv}$ (5.3‰), with dashed lines representing the expected error. Based on these ^{18}O constraints, the range of J_{riv}/J_{bio} is constrained to >2.0 ($\log(J_{riv}/J_{bio})$>0.30).

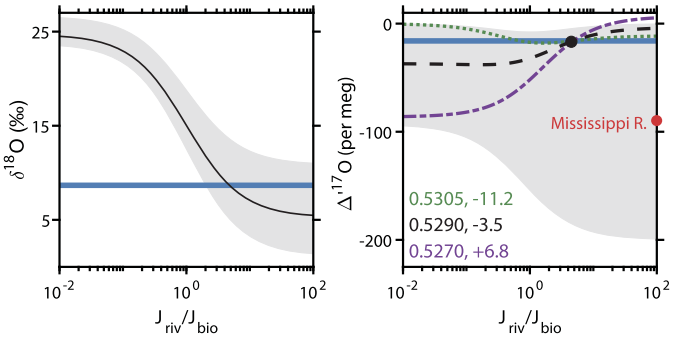

Fig. 4. The gray area represents the full space of model solutions for seawater sulfate $\delta^{18}O$ (left panel) and $\Delta'^{17}O$ (right panel), where no constraints are placed on the flux sizes (J_{riv}/J_{bio}, x-axes). The horizontal blue lines represent modern seawater sulfate values ($\delta^{18}O$ = 8.67 ± 0.21‰ and $\Delta'^{17}O$ = −16 ± 17 per meg, respectively). In the left panel, the black curve represents a unique model solution, when $\delta^{18}O_{riv}$ = 5.3‰ and $\delta^{18}O_{bio}$ = 25.0‰. The curve crosses modern seawater sulfate composition at J_{riv}/J_{bio} = 4.8. This curve corresponds to the three lines in the right panel, which represent $\Delta'^{17}O$ of seawater sulfate. The red point indicates $\Delta'^{17}O_{riv}$ = −90 per meg, to reflect average Mississippi River sulfate composition (see Fig. S5). The three lines are adjusted so that J_{riv}/J_{bio} is equal to 4.8, as predicted from the left panel, and their corresponding $\Delta'^{17}O_{riv}$ are close to 0 per meg (indicating that no anomaly is present).

Oxidative weathering in terrestrial environments may impart a mass-independent isotope anomaly into riverine sulfate that is not apparent in ^{18}O alone, but is when ^{17}O measurements are included. Marine biological recycling may dampen the anomaly, depending on the deviation of θ from θ_{RL} = 0.5305. Unlike the ^{18}O treatment of sulfate, where rich riverine datasets are available and both models and data exist for microbial systems, the ^{17}O predictions are less constrained. Here we consider the range of possible magnitudes of the mass-independent anomaly incorporated into riverine sulfate and of the specific mass-dependent mass law(s) that govern microbial recycling.

Loose constraints can be placed on ^{17}O contributions. In the case of modern riverine inputs, measurements from the Mississippi River record a strongly negative composition, ranging from −200

to 0 per meg (Killingsworth et al., 2018). This value will be revised as global riverine estimates improve, but serves as a useful first-order target for the composition of rivers. (Later, we consider the link between this composition and atmospheric O_2/CO_2.) For the microbial contributions, this process should be governed by a mass-dependent mass law, or $^{17}\theta_{bio}$, which is taken to be similar to other more well-constrained systems, i.e., values of ≈0.5285 (see Section 5.2), with variability of 0.0026. With this, we investigate the sensitivity of marine sulfate $\Delta'^{17}O$ to J_{riv}/J_{bio} as a function of $\Delta'^{17}O_{riv}$ and $\Delta'^{17}O_{bio}$. The $\Delta'^{17}O_{bio}$ term is a product of θ and the magnitude of the microbial $\delta^{18}O_{bio}$. In Fig. 4 in the right panel, the left intercept is again the microbial component, with the value range for $\Delta'^{17}O$ reflecting variable θ values (0.527-0.5305) combined with the range of $\delta^{18}O_{bio}$ (24-27‰). Similarly, the right intercept captures the range of river $\Delta'^{17}O$ values (−200 to 0 per meg). With further refinement of the global $\Delta'^{17}O$ of riverine sulfate, the model can predict a flux balance (J_{riv}/J_{bio}). Interestingly, if we apply an average $J_{riv}/J_{bio} = 4.8$ to the ^{17}O mixing calculation, the resulting $\Delta'^{17}O_{riv}$ ranges from −4 to 33 per meg, depending on the choice of θ_{bio} (0.527-0.5305) (see Fig. 4). This suggests that the Mississippi River value is not globally representative.

We also consider that the $\Delta'^{17}O$ of modern sulfate may reflect a purely mass-dependent signal. For example, the measured $\delta^{18}O$ and $\Delta'^{17}O$ could be generated by microbial processes that fractionate sulfate by $^{18}\alpha = 1.00867$ and with a mass-dependent relationship given by $\theta = 0.5285$, to agree with seawater sulfate composition. However, given the range of $\delta^{18}O_{bio}$ predicted from our sulfur metabolism studies, this is not likely for ^{18}O. Here, the isotope composition of seawater sulfate remains a balance between riverine sulfate inputs that contribute sulfate with lighter $\delta^{18}O$, and microbially cycled sulfate imparting more enriched $\delta^{18}O$.

6.1. Traditional sulfide oxidation

At high rates of cell-specific sulfate reduction, traditional sulfide oxidation is a significant sulfate generating flux. Estimates of the proportion of hydrogen sulfide produced in typical sediments that is reoxidized via sulfide oxidation and disproportionation range from 40 to 90% (Masterson et al., 2016; Jørgensen, 1982, 1977). These estimates are largely considered in the absence of arguments involving cell-specific sulfate reduction rates, and forwarded based on diagenetic grounds and radio-tracer studies. Simultaneously, when cell specific rates are high, the relative flux of sulfate that exchanges intracellularly with water decreases (to less than 20% of global sulfate reduction rate for cell specific rates of 5 fmol/cell day and above) (Bertran et al., 2019). As a consequence, the magnitude of the traditional sulfide oxidation flux outweighs that of intracellular recycling in this scenario.

For sulfide oxidation to be modeled in a meaningful way, the magnitude and composition of the flux must be known. First, as more work targets sulfate reduction, a more clear picture will emerge on cellular-scale rates of sulfate consumption, addressing the question of whether sulfide oxidation is a feasible contributor in sulfate budgets. Next, physiologically rooted constraints are needed on the isotope effects from sulfide oxidation (current estimates range from +8 to +17‰ (Turchyn and Schrag, 2004)). If sulfide reoxidation is added to the model framework presented herein, a wider range of modeled J_{riv}/J_{bio} values can satisfy modern seawater sulfate ^{18}O.

6.2. Estimates of global sulfate reduction rates

Previous studies have used local sulfate reduction data to draw inferences about the global rate of sulfate reduction. *In situ* measured reduction rates, which are posited to scale exponentially with depth, are integrated over the area of seafloor beneath highly productive zones (Turchyn and Schrag, 2006; Jørgensen, 1982, 1977). The spatial heterogeneity of sulfate reduction rates complicates this type of global estimate. In published calculations, 10% of the ocean floor at any given depth is taken to be "highly productive". This accounts for the correct observation that shallow, more nutrient-rich environments with higher sedimentation rates house much of the world's biogeochemical activity. A log-linear regression through the compiled data allows for a sense of uncertainty in such an estimate (see Fig. S3). Integrating over ocean floor area, the global sulfate reduction rate is calculated to be $8 \cdot 10^{12}$ mol/yr (Turchyn and Schrag, 2006) with an error of more than an order of magnitude. Using a dependence on depth, but leaning more heavily on sulfate concentration profiles in pore waters and applying an artificial neural network, Bowles et al. (2014) estimated that global sulfate reduction is 11.3×10^{12} moles per year. This analysis used 199 sediment profiles of pore water sulfate, and predicted sulfate metabolic rates for each cm^2 of the ocean floor by calibrating to the measured profiles. Reduction rates were then integrated over the entire ocean. In contrast to this higher value, Berner and Canfield (1989) estimated that global sulfate reduction rates were roughly 6×10^{11} moles per year. All of these estimates are then subjected to a further conversion, where we assume a generic relative sulfide re-oxidation flux f_{ox} of ≈0.8 times sulfate reduction (Jørgensen, 1982).

Here we estimate the global sulfate reduction rate using the global seawater sulfate oxygen isotope reservoir, a well-mixed pool that integrates across ocean basins. This approach is independent of local rate measurements, relies on our new conceptualization of oxygen in sulfate, and as discussed below, will further incorporate ^{17}O data. The riverine sulfate flux is known to be within $2.8 \pm 0.6 \cdot 10^{12}$ mol/yr (Burke et al., 2018) (This error is derived from the propagated errors on pyrite - σ_{py} - and sulfate weathering - σ_{sulf}, where $\sigma_{riv} = \sqrt{a_{py}^2\sigma_{py}^2 + b_{sulf}^2\sigma_{sulf}^2}$.), the biological flux is then predicted to be $< 0.8 \cdot 10^{12}$ mol/yr (based on $J_{riv}/J_{bio} > 2.2$ (see Fig. 4 left panel). To be clear, J_{bio} is the biological re-oxidation rate within sulfate reducing Bacteria and Archaea. Under environmental conditions typical of pore waters and at cellular rates < 0.2 fmol $cell^{-1}$ day^{-1} (again an expectation from pore water chemistry), predictions for F_{SO_3} range from ≈ 0.1 to 10 (see S6). This is consistent with the factor of ≈ 2 extracted from an isotope labeling study at high metabolic rates (Farquhar et al., 2008). This then equates to global net sulfate reduction rate of less than $8 \cdot 10^{12}$ mol/yr (based on $F_{SO_3} = 0.1$). This upper bound is consistent with previous global estimates of net sulfate reduction (Berner and Canfield, 1989; Turchyn and Schrag, 2006; Bowles et al., 2014).

6.3. Implications for atmospheric reconstructions

Measuring the ^{17}O-composition of barite from the geological record was popularized by (Bao et al., 2008, 2009): the ^{17}O-composition of seawater sulfate in particular has been suggested to relate to the atmospheric ratio pO_2/pCO_2. The work described herein calibrating the $\Delta'^{17}O$ in modern seawater sulfate is a direct extension of that literature, now with an expanded model framework. Our model has biogeochemistry (i.e. an ocean and river systems) underpinning previous models used to describe the atmospheric dynamics (Cao and Bao, 2013). This handling of ^{17}O includes microbial recycling and inorganic equilibrium isotope effects, all tied to the composition of seawater H_2O. Predictions for past pO_2/pCO_2 that are based on the oxygen isotope composition of seawater sulfate must now be considered in the context of the global biogeochemical sulfur cycle.

We test the sensitivity of a coupled atmospheric (Cao and Bao, 2013) and biogeochemical model, starting from a range of seawater sulfate $\Delta'^{17}O$ compositions. New variables are required that

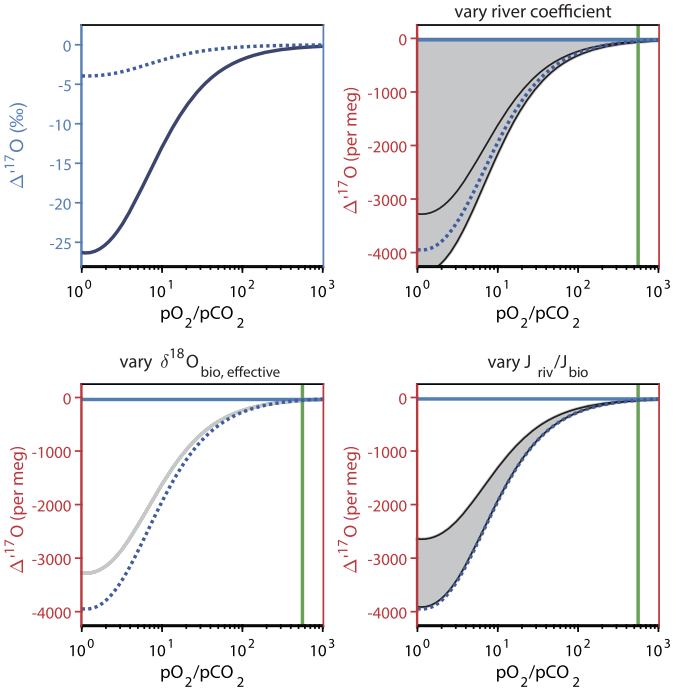

Fig. 5. This four-panel figure shows how the $\Delta'^{17}O$ of tropospheric O_2 and of sulfate (y-axes) vary as the atmospheric ratio pO_2/pCO_2 (x-axis) varies across a range reflective of Phanerozoic atmospheric compositions. (a) The $\Delta'^{17}O$ of tropospheric O_2 is a solid curve, and the $\Delta'^{17}O$ of riverine sulfate is a dotted curve, with the y-axis in blue in units of ‰. In the three subsequent panels, for which the y-axes are in red in units of per meg, the $\Delta'^{17}O$ of seawater sulfate is shown in gray relative to the $\Delta'^{17}O$ of riverine sulfate in the dotted line. The model variables in each run are held constant unless otherwise specified (river coefficient = 15%, $\delta^{18}O_{bio,\ effective}$ = 25‰, and $J_{riv}/J_{bio} = 4.8$). (b) The river coefficient, reflecting the portion of sulfate oxygen atoms that derive from atmospheric O_2, is varied between 0 and 20%. (c) The microbial ^{18}O composition, $\delta^{18}O_{bio,\ effective}$, is varied between 24 and 27‰ while $^{17}\theta_{bio}$ is held constant at 0.530. (d) The ratio J_{riv}/J_{bio} is held at >2.0, reflecting the estimate based on ^{18}O from Fig. 3. The vertical green line in each panel represents preindustrial pO_2/pCO_2 (for $pO_2 = 209500$ ppmv and $pCO_2 = 280$ ppmv). The horizontal blue line represents modern seawater sulfate $\Delta'^{17}O = -16$ per meg.

describe the magnitude of the atmospheric O_2 isotope anomaly and its uptake by rivers during weathering. The ratio of pO_2/pCO_2 carries a functional relationship to $\Delta'^{17}O$ of atmospheric O_2 (see Fig. 5) and $\Delta'^{17}O$ of atmospheric CO_2 (Cao and Bao, 2013). For each model run, pO_2/pCO_2 varies from 1 to 1000 in order to express the full range of expected Phanerozoic atmospheric compositions (Berner, 2006).

Fig. 5 demonstrates the sensitivity of the $\Delta'^{17}O$ (y-axis) composition of tropospheric O_2, riverine sulfate, and marine sulfate to pO_2/pCO_2 (x-axis). Here, the $\delta^{18}O$ of seawater sulfate is fixed at 8.67‰, along with $\delta^{18}O_{riv}$ of 5.3‰. In each of the analyses, c_{uptake}, $\delta^{18}O_{bio}$, and J_{riv}/J_{bio} are allowed to vary, respectively. Note that the modern values for marine sulfate (blue horizontal lines) and atmosphere (green vertical lines) fall to the oxidized portion of the Phanerozoic atmospheric range. The variable c_{uptake} (Fig. 5b) describes the proportion of river sulfate oxygen atoms that are derived from atmospheric O_2. Studies show that molecular oxygen constitutes a small relative fraction of a new formed sulfate molecule, ranging from 21 to 29% in laboratory experiments of pyrite oxidation (Kohl and Bao, 2011) to 5-25% for field based approaches that incorporate the pyrite:evaporite ratio in sulfate production (Killingsworth et al., 2018). We adopt a reasonable range of 0 to 20%. A similar test on δO_{bio} (Fig. 5c) and J_{riv}/J_{bio} (Fig. 5d) demonstrates the sensitivity of the $\Delta'^{17}O$ in sulfate to changes in these values. The input variability in $\delta^{18}O_{bio}$ (24-27‰) is derived from the error envelope around the mean sulfate reduction fractionation factor (Bertran et al., 2019) and assuming a $^{17}\theta_{bio}$ of 0.5285. For the flux balance analysis, the input range is taken from 2.0 to ∞.

It is clear that significantly negative $\Delta'^{17}O$ signals are uniquely related to the $\Delta'^{17}O$ composition of atmospheric O_2. It remains the case that this value is then tied to the ratio pO_2/pCO_2. Therefore the $\Delta'^{17}O$ of the geological sulfate record should provide a rich history of atmospheric compositions. Some variation in sulfate $\Delta'^{17}O$ may reflect changes in other model variables, in particular c_{uptake} (see Fig. 5b). For the two other variables $\delta^{18}O_{bio,\ effective}$ and J_{riv}/J_{bio}, the sensitivity analyses in Fig. 5c and d demonstrate that this variability is second-order to the atmospheric composition. In the preceding discussion, we have constrained each of these parameters in the modern, with the expectation that the values will not change dramatically (by orders of magnitude) on Phanerozoic timescales. The effect that variations of each parameter have on the $\Delta'^{17}O$ of seawater sulfate is captured by the gray shaded areas. It is noteworthy that the effects of individual parameters is larger at low pO_2/pCO_2. This is particularly true for c_{uptake} and J_{riv}/J_{bio}, whereas the biological isotope effects exert less of a control. Even if chosen parameters are incorrect for models of ancient sulfates, the *relative* changes between geological units or through time should still be valid.

7. Conclusions

We report new high-precision measurements characterizing the triple oxygen isotope composition of modern seawater sulfate ($\delta^{18}O$ and $\Delta'^{17}O$). This composition is modeled as arising from two sulfate-generating reactions/fluxes: riverine sulfate delivery (J_{riv}) and microbial intracellular oxidation (J_{bio}). In a departure from previous oxygen isotope models, the new biological flux describes the recycling of sulfate oxygen isotopes within sulfate-reducing microorganisms, an argument derived from quantitative observations in experimental systems (Farquhar et al., 2008) and recent cellular-scale models (Bertran et al., 2019). This analysis lends to a global picture of sulfate usage and recycling. To satisfy the modeled ^{18}O and ^{17}O abundances in seawater sulfate, the global sulfate reduction rate is constrained to be $<15.0{\cdot}10^{12}$ mol/yr, for an F_{ox} value of 0.1. This upper bound is consistent with all published estimates (Bowles et al., 2014; Turchyn and Schrag, 2004, 2006).

In describing what sets modern seawater sulfate $\delta^{18}O$ and $\Delta'^{17}O$, a quantitative understanding of the role for rivers and biology is in hand. This model allows for a refined interpretation of measurements of ancient seawater sulfate with the continued goal of identifying changes in $\Delta'^{17}O$ of atmospheric O_2, and therefore of pCO_2/pO_2.

Appendix A. Supplementary material

Supplementary material related to this article can be found online at https://doi.org/10.1016/j.epsl.2019.06.013.

References

Antler, G., Turchyn, A.V., Herut, B., Sivan, O., 2015. A unique isotopic fingerprint of sulfate-driven anaerobic oxidation of methane. Geology 43 (7), 619–622.

Antler, G., Turchyn, A.V., Rennie, V., Herut, B., Sivan, O., 2013. Coupled sulfur and oxygen isotope insight into bacterial sulfate reduction in the natural environment. Geochim. Cosmochim. Acta 118, 98–117.

Bao, H.M., Fairchild, I.J., Wynn, P.M., Spotl, C., 2009. Stretching the envelope of past surface environments: neoproterozoic glacial lakes from svalbard. Science 323 (5910), 119–122.

Bao, H.M., Lyons, J.R., Zhou, C.M., 2008. Triple oxygen isotope evidence for elevated CO_2 levels after a neoproterozoic glaciation. Nature 453 (7194), 504–506.

Barkan, Eugeni, Luz, Boaz, 2005. High precision measurements of $^{17}O/^{16}O$ and $^{18}O/^{16}O$ ratios in H_2O. Rapid Commun. Mass Spectrom. 19 (24), 3737–3742.

Bergman, Noam M., Lenton, Timothy M., Watson, Andrew J., 2004. Copse: a new model of biogeochemical cycling over Phanerozoic time. Am. J. Sci. 304 (5), 397–437.
Berner, Elizabeth Kay, Berner, Robert A., 2012. Global Environment: Water, Air, and Geochemical Cycles. Princeton University Press.
Berner, R.A., Canfield, D.E., 1989. A new model for atmospheric oxygen over Phanerozoic time. Am. J. Sci. 289 (4), 333–361.
Berner, Robert A., 2006. Geocarbsulf: a combined model for Phanerozoic atmospheric O_2 and CO_2. Geochim. Cosmochim. Acta 70 (23), 5653–5664.
Bertran, E., Waldeck, A., Wing, B.A., Halevy, I., Leavitt, W.D., Bradley, A.S., Johnston, D.T., 2019. Oxygen isotope effects during microbial sulfate reduction: applications to sediment cell abundance. In preparation.
Böttcher, Michael E., Thamdrup, B., Vennemann, Torsten W., 2001. Oxygen and sulfur isotope fractionation during anaerobic bacterial disproportionation of elemental sulfur. Geochim. Cosmochim. Acta 65 (10), 1601–1609.
Böttcher, Michael E., Thamdrup, Bo, 2001. Anaerobic sulfide oxidation and stable isotope fractionation associated with bacterial sulfur disproportionation in the presence of MnO2. Geochim. Cosmochim. Acta 65 (10), 1573–1581.
Bowles, Marshall W., Mogollón, José M., Kasten, Sabine, Zabel, Matthias, Hinrichs, Kai-Uwe, 2014. Global rates of marine sulfate reduction and implications for sub–sea-floor metabolic activities. Science, 1249213.
Brunner, Benjamin, Bernasconi, Stefano M., 2005. A revised isotope fractionation model for dissimilatory sulfate reduction in sulfate reducing bacteria. Geochim. Cosmochim. Acta 69 (20), 4759–4771.
Burke, Andrea, Present, Theodore M., Paris, Guillaume, Rae, Emily C.M., Sandilands, Brodie H., Gaillardet, Jérôme, Peucker-Ehrenbrink, Bernhard, Fischer, Woodward W., McClelland, James W., Spencer, Robert G.M., et al., 2018. Sulfur isotopes in rivers: insights into global weathering budgets, pyrite oxidation, and the modern sulfur cycle. Earth Planet. Sci. Lett. 496, 168–177.
Canfield, D.E., 1991. Sulfate reduction in deep-sea sediments. Am. J. Sci. 291 (2), 177–188.
Canfield, D.E., 2004. The evolution of the Earth surface sulfur reservoir. Am. J. Sci. 304 (10), 839–861.
Canfield, Don E., Stewart, Frank J., Thamdrup, Bo, De Brabandere, Loreto, Dalsgaard, Tage, Delong, Edward F., Revsbech, Niels Peter, Ulloa, Osvaldo, 2010. A cryptic sulfur cycle in oxygen-minimum–zone waters off the Chilean coast. Science 330 (6009), 1375–1378.
Cao, X.B., Bao, H.M., 2013. Dynamic model constraints on oxygen-17 depletion in atmospheric O_2 after a snowball earth. Proc. Natl. Acad. Sci. USA 110 (36), 14546–14550.
Cao, Xiaobin, Liu, Yun, 2011. Equilibrium mass-dependent fractionation relationships for triple oxygen isotopes. Geochim. Cosmochim. Acta 75 (23), 7435–7445.
Cowie, B.R., Johnston, D.T., 2016. High-precision measurement and standard calibration of triple oxygen isotopic compositions (delta O-18, delta 'O-17) of sulfate by f-2 laser fluorination. Chem. Geol. 440, 50–59.
Crockford, P.W., Cowie, B.R., Johnston, D.T., Hoffman, P.F., Sugiyama, I., Pellerin, A., Bui, T.H., Hayles, J., Halverson, G.P., Macdonald, F.A., Wing, B.A., 2016. Triple oxygen and multiple sulfur isotope constraints on the evolution of the post-Marinoan sulfur cycle. Earth Planet. Sci. Lett. 435, 74–83.
D'Hondt, S., Rutherford, S., Spivack, A.J., 2002. Metabolic activity of subsurface life in deep-sea sediments. Science 295 (5562), 2067–2070.
Farquhar, James, Canfield, Don E., Masterson, Andrew, Bao, Huiming, Johnston, David, 2008. Sulfur and oxygen isotope study of sulfate reduction in experiments with natural populations from Faellestrand, Denmark. Geochim. Cosmochim. Acta 72 (12), 2805–2821.
Fritz, P., Basharmal, G.M., Drimmie, R.J., Ibsen, J., Qureshi, R.M., 1989. Oxygen isotope exchange between sulphate and water during bacterial reduction of sulphate. Chem. Geol., Isot. Geosci. Sect. 79 (2), 99–105.
Fry, Brian, Ruf, William, Gest, Howard, Hayes, J.M., 1988. Sulfur isotope effects associated with oxidation of sulfide by O_2 in aqueous solution. Chem. Geol., Isot. Geosci. Sect. 73 (3), 205–210.
Halevy, Itay, Peters, Shanan E., Fischer, Woodward W., 2012. Sulfate burial constraints on the Phanerozoic sulfur cycle. Science 337 (6092), 331–334.
Hayes, J.M., Waldbauer, J.R., 2006. The carbon cycle and associated redox processes through time. Philos. Trans. R. Soc. Lond. B, Biol. Sci. 361 (1470), 931–950.
Hoehler, Tori M., Jørgensen, Bo Barker, 2013. Microbial life under extreme energy limitation. Nat. Rev. Microbiol. 11 (2), 83.
Holser, William T., Kaplan, Isaac R., Sakai, Hitoshi, Zak, Israel, 1979. Isotope geochemistry of oxygen in the sedimentary sulfate cycle. Chem. Geol. 25 (1–2), 1–17.
Johnston, D.T., Gill, B.C., Masterson, A., Beirne, E., Casciotti, K.L., Knapp, A.N., Berelson, W., 2014. Placing an upper limit on cryptic marine sulphur cycling. Nature 513 (7519), 530–533.
Jørgensen, Bo Barker, 1977. The sulfur cycle of a coastal marine sediment (Limfjorden, Denmark) 1. Limnol. Oceanogr. 22 (5), 814–832.
Jørgensen, Bo Barker, 1982. Mineralization of organic matter in the sea bed—the role of sulphate reduction. Nature 296 (5858), 643.
Killingsworth, Bryan A., Bao, Huiming, Kohl, Issaku E., 2018. Assessing pyrite-derived sulfate in the Mississippi River with four years of sulfur and triple-oxygen isotope data. Environ. Sci. Technol. 52 (11), 6126–6136.
Kohl, Issaku, Bao, Huiming, 2011. Triple-oxygen-isotope determination of molecular oxygen incorporation in sulfate produced during abiotic pyrite oxidation (pH = 2–11). Geochim. Cosmochim. Acta 75 (7), 1785–1798.
Landais, Amaelle, Barkan, Eugeni, Luz, Boaz, 2008. Record of $\delta^{18}O$ and ^{17}O-excess in ice from vostok Antarctica during the last 150,000 years. Geophys. Res. Lett. 35 (2).
Leavitt, William D., Halevy, Itay, Bradley, Alexander S., Johnston, David T., 2013. Influence of sulfate reduction rates on the Phanerozoic sulfur isotope record. Proc. Natl. Acad. Sci. 110 (28), 11244–11249.
Leloup, Julie, Fossing, Henrik, Kohls, Katharina, Holmkvist, Lars, Borowski, Christian, Jørgensen, Bo Barker, 2009. Sulfate-reducing bacteria in marine sediment (Aarhus Bay, Denmark): abundance and diversity related to geochemical zonation. Environ. Microbiol. 11 (5), 1278–1291.
Levin, Naomi E., Raub, Timothy D., Dauphas, Nicolas, Eiler, John M., 2014. Triple oxygen isotope variations in sedimentary rocks. Geochim. Cosmochim. Acta 139, 173–189.
Masterson, A.L., Wing, B.A., Paytan, A., Farquhar, J., Johnston, D.T., 2016. The minor sulfur isotope composition of Cretaceous and Cenozoic seawater sulfate. Paleoceanography 31 (6), 779–788.
Meybeck, Michel, 1979. Concentrations des eaux fluviales en elements majeurs et apports en solution aux oceans. Rev. Géol. Dyn. Géogr. Phys. 21 (3), 215–246.
Miller, M.F., 2002. Isotopic fractionation and the quantification of O-17 anomalies in the oxygen three-isotope system: an appraisal and geochemical significance. Geochim. Cosmochim. Acta 66 (11), 1881–1889.
Müller, Inigo A., Brunner, Benjamin, Breuer, Christian, Coleman, Max, Bach, Wolfgang, 2013. The oxygen isotope equilibrium fractionation between sulfite species and water. Geochim. Cosmochim. Acta 120, 562–581.
Niewohner, C., Hensen, C., Kasten, S., Zabel, M., Schulz, H.D., 1998. Deep sulfate reduction completely mediated by anaerobic methane oxidation in sediments of the upwelling area off Namibia. Geochim. Cosmochim. Acta 62 (3), 455–464.
Pack, Andreas, Herwartz, Daniel, 2014. The triple oxygen isotope composition of the Earth mantle and understanding variations in terrestrial rocks and minerals. Earth Planet. Sci. Lett. 390, 138–145.
Paytan, A., Kastner, M., Campbell, D., Thiemens, M.H., 1998. Sulfur isotopic composition of Cenozoic seawater sulfate. Science 282 (5393), 1459–1462.
Paytan, A., Kastner, M., Campbell, D., Thiemens, M.H., 2004. Seawater sulfur isotope fluctuations in the Cretaceous. Science 304 (5677), 1663–1665.
Rennie, Victoria C.F., Turchyn, Alexandra V., 2014. Controls on the abiotic exchange between aqueous sulfate and water under laboratory conditions. Limnol. Oceanogr., Methods 12, 166–173.
Thamdrup, B., Fossing, H., Jorgensen, B.B., 1994. Manganese, iron, and sulfur cycling in a coastal marine sediment, Aarhus Bay, Denmark. Geochim. Cosmochim. Acta 58 (23), 5115–5129.
Tichomirowa, Marion, Junghans, Manuela, 2009. Oxygen isotope evidence for sorption of molecular oxygen to pyrite surface sites and incorporation into sulfate in oxidation experiments. Appl. Geochem. 24 (11), 2072–2092.
Turchyn, A.V., Schrag, D.P., 2006. Cenozoic evolution of the sulfur cycle: insight from oxygen isotopes in marine sulfate. Earth Planet. Sci. Lett. 241 (3–4), 763–779.
Turchyn, Alexandra V., Brüchert, Volker, Lyons, Timothy W., Engel, Gregory S., Balci, Nurgul, Schrag, Daniel P., Brunner, Benjamin, 2010. Kinetic oxygen isotope effects during dissimilatory sulfate reduction: a combined theoretical and experimental approach. Geochim. Cosmochim. Acta 74 (7), 2011–2024.
Turchyn, Alexandra V., Schrag, Daniel P., 2004. Oxygen isotope constraints on the sulfur cycle over the past 10 million years. Science 303 (5666).
Van Stempvoort, D.R., Krouse, H.R., 1994. Controls of $D^{18}O$ in Sulfate. ACS Publications.
Wankel, S.D., Bradley, A.S., Eldridge, D.L., Johnston, D.T., 2014. Determination and application of the equilibrium oxygen isotope effect between water and sulfite. Geochim. Cosmochim. Acta 125, 694–711.
Wing, B.A., Halevy, I., 2014. Intracellular metabolite levels shape sulfur isotope fractionation during microbial sulfate respiration. Proc. Natl. Acad. Sci. USA 111 (51), 18116–18125.
Wortmann, Ulrich G., Chernyavsky, Boris, Bernasconi, Stefano M., Brunner, Benjamin, Böttcher, Michael E., Swart, Peter K., 2007. Oxygen isotope biogeochemistry of pore water sulfate in the deep biosphere: dominance of isotope exchange reactions with ambient water during microbial sulfate reduction (ODP Site 1130). Geochim. Cosmochim. Acta 71 (17), 4221–4232.
Young, Edward D., Galy, Albert, Nagahara, Hiroko, 2002. Kinetic and equilibrium mass-dependent isotope fractionation laws in nature and their geochemical and cosmochemical significance. Geochim. Cosmochim. Acta 66 (6), 1095–1104.
Young, Edward D., Yeung, Laurence Y., Kohl, Issaku E., 2014. On the $\Delta^{17}O$ budget of atmospheric O_2. Geochim. Cosmochim. Acta 135, 102–125.
Zeebe, Richard E., 2010. A new value for the stable oxygen isotope fractionation between dissolved sulfate ion and water. Geochim. Cosmochim. Acta 74 (3), 818–828.
Zeebe, Richard E., Wolf-Gladrow, Dieter A., 2001. CO2 in Seawater: Equilibrium, Kinetics, Isotopes. Gulf Professional Publishing.